Atmos. Meas. Tech. Discuss., https://doi.org/10.5194/amt-2017-402
Manuscript under review for journal Atmos. Meas. Tech.
Discussion started: 22 December 2017

Atmospheric Measurement Techniques Discussions

Cloud classification of ground-based infrared images combining manifold and texture features

Qixiang Luo[1], Yong Meng[1], Lei Liu[1], Xiaofeng Zhao[1], and Zeming Zhou[1]

[1]College of Meteorology and Oceanology, National University of Defense Technology, Nanjing, 211101, China

Correspondence to: Zeming Zhou (zhou_zeming@yahoo.com)

Abstract. Automatic cloud type recognition of ground-based infrared images is still a challenging task. A novel cloud classification method is proposed to group images into five cloud types based on manifold and texture features. Compared with statistical features in the Euclidean space, manifold features extracted on Symmetric Positive Definite (SPD) matrix space can describe the non-Euclidean geometric characteristics of the infrared image. The proposed method comprises three stages: pre-processing, feature extraction and classification. Cloud classification is performed by the Support Vector Machine (SVM). The datasets are comprised of the zenithal and whole-sky images taken by the Whole-Sky Infrared Cloud-Measuring System (WSIRCMS). Benefiting from the joint features, compared to the recent cloud type recognition methods, the experimental results illustrate that the proposed method acquires a higher recognition rate and exhibits a more competitive classification result on the ground-based infrared datasets.

1. Introduction

The cloud has an essential impact on the absorption, scattering, emission of atmosphere, the vertical transport of heat, moisture and momentum (Hartmann et al., 1992; Chen et al., 2000). Cloud cover and cloud type can affect the daily weather and climate change through its radiation and hydrological effects (Isaac and Stuart, 1996; Liu et al., 2008; Naud et al., 2016). Therefore, accurate cloud detection and classification is necessary for meteorological observation. Nowadays, cloud cover changes and cloud type determination have been available through the ground-based sky imaging systems (Souzaecher et al., 2006; Shields et al., 2003). Different from traditional manual observation, sky-imaging devices can obtain continuous information of sky condition at a local scale with a high spatial resolution.

However, due to subject factors and a rough measuring system, the estimation of cloud cover and type may weaken their credibility (Tzoumanikas et al., 2012). Some attempts have been made to develop algorithms for cloud classification of ground-based images (Buch and Sun, 2005; Singh and Glennen, 2005; Cazorla et al., 2008; Heinle et al., 2010; Ghonima et al., 2012; Taravat et al., 2014; Zhuo et al., 2014). Wang and Sassen (2001) developed a cloud detection algorithm by combining ground-based active and passive remote sensing data to illustrate how extended-time remote sensing datasets can be converted to cloud properties of concern to climate research. Li et al. (2002) proposed a method for automatic classification of surface and cloud type using Moderate Resolution Imaging Spectro-radiometer (MODIS) radiance measurements, whose advantage lied in its independence of radiance or brightness temperature threshold criteria, and its

interpretation of each class was based on the radiative spectral characteristics of different classes. Singh and Glennen (2005) adopted the k-nearest neighbour (KNN) and neural network classifiers to identify cloud types with texture features, including autocorrelation, co-occurrence matrices, edge frequency, Law's features and primitive length. Calbó and Sabburg (2008) extracted statistical texture features based on the greyscale images, pattern features based on the spectral power function of images and other features based on the thresholded images for recognizing the cloud type with the supervised parallelepiped classifier. Heinle et al. (2010) chose 12 dimensional features mainly describing the colour and the texture of images for automatic cloud classification, based on the KNN classifier. Besides the statistical feature like the mean grey value of the infrared image, Liu et al. (2011) explored another six structure features to characterize the cloud structure for classification. Zhuo et al. (2014) validated that cloud classification may not perform well if the texture or structure features were employed alone. As a result, texture and structure features were captured from the colour image and then fed into a trained Support Vector Machine (SVM) to obtain the cloud type. Different from traditional feature extraction, Shi et al. (2017) proposed to adopt the deep convolutional activations-based features and provided a promising cloud type recognition result with a multi-label linear SVM model.

Automatic cloud classification has made certain achievements; however, the cloud classification of ground-based infrared images poses a great challenge to us. By far, few research works of cloud classification have been dedicated to the ground-based infrared images (Sun et al., 2009; Liu et al., 2011). Ground-based infrared images can be obtained continuously day and night but lack colour information, so it's hard to reach a perfect performance when the recognition method of colour images is applied to the infrared images. Most recent methods conducted on the RGB visible images (Heinle et al., 2010; Zhuo et al., 2014; Li et al., 2016; Gan et al., 2017) cannot directly be exploited on the cloud type classification of infrared images owing to the lack of colour information.

Nowadays, the Symmetric Positive Definite (SPD) matrix manifold has achieved success in many aspects, such as action recognition, material classification and image segmentation (Faraki et al., 2015; Jayasumana et al., 2015). Although it proves effective, few researches are pursued for the task of cloud classification with manifold features. In this paper, a novel cloud classification method combining manifold and texture features is proposed for ground-based infrared images.

To exhibit the classification performance, we have compared the results with the other two models (Liu et al., 2015; Cheng and Yu, 2015), which are adapted for the classification task of infrared images. To make up for the weakness of the Local Binary Patterns (LBP) that cannot describe the local contrast well, Liu et al. (2015) proposed a new descriptor called Weighted Local Binary Patterns (WLBP) for the feature extraction. And then the KNN classifier based on the chi-square distance was employed for cloud type recognition. Cheng and Yu (2015) incorporated statistical features and local texture features for block-based cloud classification. As Cheng and Yu (2015) reported, the method combining the statistical and uniform LBP features with the Bayesian classifier (Bensmail and Celeux, 1996) displayed the best performance in the 10-fold cross validation overall.

In this paper, the data and methodology of the method are described in Sect. 2. Section 3 focuses on the experimental results. Conclusions are summarized in Sect. 4.

Atmos. Meas. Tech. Discuss., https://doi.org/10.5194/amt-2017-402
Manuscript under review for journal Atmos. Meas. Tech.
Discussion started: 22 December 2017

2. Data and Methodology

In this section, the datasets and the methodology for cloud classification are introduced. The proposed method contains three main steps: pre-processing, feature extraction and classification. The framework is illustrated in Fig. 1.

2.1 Dataset and pre-processing

The datasets include the zenithal images and whole-sky images, which are gathered by the Whole-Sky Infrared Cloud Measurement System (WSIRCMS) (Liu et al., 2013). The WSIRCMS is a ground-based passive system that an uncooled microbolometer detector array of 320×240 pixels is used to measure downwelling atmospheric radiance in 8-14μm (Liu et al., 2011). A whole-sky image is obtained after combining the zenithal image and other images at eight different orientations. As a result, the zenithal image has a resolution of 320×240 pixels while the whole-sky image is of 650×650 pixels. The datasets are provided by National University of Defense Technology in Nanjing, China.

The cloud images used in the experiment are selected with the help of two professional meteorological observers with many years of observation experiences. The selection criterion is that the chosen images should hold high visual quality and can be recognized by visual inspection. All infrared cloud images are labelled to construct the training set and testing set. To guarantee the golden-standard's confidence, only images labelled same by two meteorological observers are finally chosen as the dataset used in this study. Different from traditional cloud classification by observers, automatic cloud classification by the devices needs a new criterion for recognition. According to the morphology and generating mechanism of the cloud, the sky condition is classified into five categories in this study (Sun et al., 2009): stratiform clouds, cumuliform clouds, waveform clouds, cirriform clouds and clear sky. The sky condition and its corresponding description are as shown in Table 1.

The zenithal dataset used in this study is selected from historical dataset purposely to avoid a complex mixture of cloud types. The typical samples from each category are demonstrated in Fig. 2. As listed in Table 2, the zenithal dataset is comprised of 100 cloud images each category.

The whole-sky dataset is obtained during July to October in 2014 at Changsha, China. Since the whole-sky image is obtained by combining the nine sub-images at different orientations, the division rules of the whole-sky dataset remain the same as that of the zenithal dataset. The whole-sky samples from each category are exhibited in Fig. 3. As listed in Table 2, the number of stratiform clouds, cumuliform clouds, waveform clouds, cirriform clouds and clear sky is 246, 240, 239, 46 and 88, respectively.

As Fig. 3 shows, a pre-processing mask is provided on the whole-sky images, which is used to extract the region of interest (ROI) from the images, which is the areas of the clouds rather than the parts out of the circle. Different from the whole-sky images, all parts of the zenithal images are ROI. Thus, we implement the feature extraction directly on the original zenithal images.

Atmos. Meas. Tech. Discuss., https://doi.org/10.5194/amt-2017-402
Manuscript under review for journal Atmos. Meas. Tech.
Discussion started: 22 December 2017

Atmospheric Measurement Techniques Discussions

2.2 Feature extraction

In addition to the manifold features proposed in this work, the texture features are also combined. The manifold features of the ground-based infrared image are extracted on the SPD matrix manifolds, and after that, they are mapped into the tangent space to form a feature vector in Euclidean space. The texture features represent the statistical information in Euclidean space; on the contrary, the manifold features describe the non-Euclidean geometric characteristics of the infrared image.

2.2.1 Texture features

In this paper, the Grey Level Co-occurrence Matrix (GLCM) is used to extract the texture features, including energy, entropy, contrast and homogeneity (Haralick et al., 1973). Each matrix element in the GLCM represents the joint probability occurrence $p(i,j)$ of pixel pairs with a defined direction θ and a pixel distance d having grey level values i and j in the image.

$$\mathrm{GLCM} = \begin{bmatrix} p(0,0) & p(0,1) & p(0,2) & \dots & p(0,k-1) \\ p(1,0) & p(1,1) & p(1,2) & \dots & p(1,k-1) \\ \vdots & \vdots & \vdots & \dots & \vdots \\ p(k-1,0) & p(k-1,1) & p(k-1,2) & \dots & p(k-1,k-1) \end{bmatrix}_{k\times k} \quad (1)$$

The energy measures the uniformity and texture roughness of the grey level distribution:

$$\mathrm{Energy} = \sum_{i=0}^{k-1}\sum_{j=0}^{k-1} p(i,j)^2 \quad (2)$$

The entropy is a measure of randomness of grey level distribution:

$$\mathrm{Entropy} = -\sum_{i=0}^{k-1}\sum_{j=0}^{k-1} p(i,j)\log_2 p(i,j) \quad (3)$$

The contrast is a measure of local variation of grey level distribution:

$$\mathrm{Contrast} = \sum_{i=0}^{k-1}\sum_{j=0}^{k-1} (i-j)^2 p(i,j)^2 \quad (4)$$

The homogeneity measures the closeness of the distribution of elements in the GLCM to the GLCM diagonal:

$$\mathrm{Homogeneity} = \sum_{i=0}^{k-1}\sum_{j=0}^{k-1} \frac{p(i,j)}{1+|i-j|} \quad (5)$$

As the number of intensity levels k increases, the computation of the GLCM increases strongly. In this work, k is set with 16 and then the texture features are obtained by calculating the GLCM with $\mathrm{d} = 1$ and $\theta = 0°, 45°, 90°, 135°$. To avoid the complexity and reduce the dimension, mean values in four directions are obtained as the texture features. In the experiments, we find that these texture features are significant for the cloud classification of the ground-based infrared image.

2.2.2 Manifold features

The manifold features are attained by two steps: computing the regional Covariance Descriptor (CovD) and mapping the CovD into its tangent space to form a feature vector.

Step 1: Computing the regional CovD

Atmos. Meas. Tech. Discuss., https://doi.org/10.5194/amt-2017-402
Manuscript under review for journal Atmos. Meas. Tech.
Discussion started: 22 December 2017

Atmospheric Measurement Techniques Discussions

Suppose the image I is of the size $W \times H$, its d-dimensional features containing greyscale and gradient at each pixel are computed, which compose the feature image F, whose size is $W \times H \times d$:

$$F(x,y) = f(I,x,y) \tag{6}$$

where the feature mapping f is defined as:

$$f = \left[I(x,y) \;\; |I_x| \;\; |I_y| \;\; \sqrt{|I_x|^2 + |I_y|^2} \;\; |I_{xx}| \;\; |I_{yy}| \right]^{\mathrm{T}} \tag{7}$$

In which (x,y) denotes the location, $I(x,y)$ denotes the greyscale. $|I_x|$, $|I_y|$, $|I_{xx}|$ and $|I_{yy}|$ represent the first and second order derivative in the direction of x and y at each pixel, respectively. $\sqrt{|I_x|^2 + |I_y|^2}$ denotes the modulus of gradient.

For the feature image F, supposing it contains $n = W \times H$ points of d-dimensional features $\{f_k, k = 1,2,\dots,n\}$. Its CovD is a $d \times d$ covariance matrix, computed by Eq. (8):

$$C = \frac{1}{n-1}\sum_{k=1}^{n}(f_k - \mu)(f_k - \mu)^{\mathrm{T}} \tag{8}$$

where $\mu = \frac{1}{n}\sum_{k=1}^{n} f_k$, which represents the feature mean vector.

The CovD can fuse multiple dimensional features of the image and express the correlations between different features. It removes the mean of the sample features; therefore, it has certain effects of denoising. The CovD is symmetric and its dimension is only $d(d+1)/2$. If we convert the CovD into a feature vector to describe the image, its dimension is $n \times d$, which needs a high computation cost for cloud classification.

Step 2: Obtaining the feature vector by mapping the CovD into its tangent space

Generally speaking, the manifold is a topological space that is locally equivalent to a Euclidean space. The differential manifold has a globally defined differential structure. Its tangent space $T_X M$ is a space formed by all possible tangent vectors at a given point X on the differential manifold. For the Riemannian manifold M, an inner product is defined in its tangent space. The shortest curve between two points on the manifold is called the geodesic and the length of the geodesic is the distance between two points.

All SPD matrices form a Riemannian manifolds. Suppose S^d is a set of all $n \times n$ real symmetric matrices: $S^d = \{A \in M(d): A^{\mathrm{T}} = A\}$, where $M(d)$ represents the set of all $d \times d$ matrices, so that $S_{++}^d = \{A \in S^d : A > 0\}$ is the set of all $d \times d$ SPD matrices, which construct a $d(d+1)/2$ dimensional SPD manifold. According to the operation rules of the matrix, the set of the real symmetric matrix is a vector space while the real SPD matrix space is a non-Euclidean space. A Riemannian metric should be given to describe the geometric structure of the SPD matrix and to measure the distance of two points on S_{++}^d.

Based on the bi-invariant Riemannian metric (Arsigny et al., 2008), the distance between A and B on the SPD matrix manifold is $d(A,B) = \|\log(A) - \log(B)\|_2$, where $\log(\cdot)$ denotes matrix logarithm. The logarithmic operation is applied in the elements of the diagonal matrix obtained by the singular value decomposition of the SPD matrix.

Atmos. Meas. Tech. Discuss., https://doi.org/10.5194/amt-2017-402
Manuscript under review for journal Atmos. Meas. Tech.
Discussion started: 22 December 2017

The logarithmic operator is valid only if the eigenvalues of the symmetric matrix are positive. When no cloud is observed in the clear sky, the CovD of the image features could be non-negative definite, and in this case, it needs to be converted to a SPD matrix. We can formulate it as an optimization problem (Harandi et al., 2015):

$$\min_{A} \|C - A\|_F \quad \text{s.t. } A + A^T > 0 \tag{9}$$

where C is a CovD and A is the closest SPD matrix to C.

For a SPD matrix A, its corresponding feature vector can be represented as Eq. (10):

$$a = Vec(\log(A)) \tag{10}$$

where $Vec(B)$ is a vector in Euclidean space by vectorizing the upper triangular matrix B:

$$Vec(B) = \left[b_{1,1}, \sqrt{2}b_{1,2}, \cdots, \sqrt{2}b_{1,d}, b_{2,2}, \sqrt{2}b_{2,3}, \cdots, b_{d,d}\right]^{\mathrm{T}} \tag{11}$$

Since f is a 6-dimensional feature mapping, the manifold feature vector a to describe the cloud image is 21 dimensions.

2.2.3 Combining manifold and texture features

As described in Sect. 2.2.1 and 2.2.2, manifold and texture features can be extracted and integrated to represent the ground-based infrared images. Besides the 4-dimensional texture features, the joint features of the infrared image have a total of 25 dimensions.

2.3 Classification

The classifier used in this paper is the SVM, which exhibits prominent classification performance in the cloud type recognition experiments. It is a two-class classifier; its basic model is a linear classifier with the largest margin in the feature space. The margin maximization can be formulated as a convex quadratic programming problem. A simple linear function is chosen as the mapping kernel, which is validated by the cloud classification experiments.

For multiple-classification task, the SVM is conducted between every two classes. If there are c types, then the total number of classification operation is $c(c-1)/2$. c is set with 5 in this paper and the final result is determined by a voting policy.

3. Experiments and discussions

In this section, we report experimental results and assess the performance of the proposed cloud classification method. We first validate the effects of the proposed features by conducting each experiment 50 times on two datasets, respectively. The results of 10-fold cross validation with different features are given in Table 3. Each dataset is divided into 10 subsets with the same size at random. One single subset is used for validation and the other 9 parts are taken as the training set. As Table 3 illustrates, the overall accuracy of texture, manifold and combined features achieves 83.49%, 96.46% and 96.50% on the zenthial dataset while 78.01%, 82.38% and 85.12% on the whole-sky dataset, respectively. It can been seen that the texture

or manifold features alone don't achieve a better performance than the joint features, which not only inherit the advantage of the texture features, but also own the characteristic of manifold features. On the whole, the method using the joint features performs best in the cross validation.

Naturally, combined features are used for the cloud type recognition. In the experiment, each dataset is grouped into the training set and testing set. The training set is selected randomly from each category in accordance with a certain proportion 1/10, 1/2 and 9/10, respectively and the rest part forms the testing set. Each experiment is implemented 50 times and the average accuracy is regarded as the final results of classification.

To exhibit the recognition performance of the proposed method, we also compare with the other two models (Liu et al., 2015; Cheng and Yu, 2015) to assess its performance in this experiment. Liu's model employs WLBP feature with the KNN classifier based on the chi-square distance while Cheng's method adopts the statistical and uniform LBP features with the Bayesian classifier. Note that we extract the statistical features from the greyscale images rather than from the RGB images so that the statistical features have only 8 dimension, as a result, without extra colour information provided, both of the two methods are adaptable to the infrared images.

3.1 Results of the zenithal dataset

The first experiment is performed on the zenithal dataset. Tabel 4 reports the overall recognition rates of the proposed method and the other methods. The proposed method gets the best results, with at least 2.5% improvement over Liu's method and over 9.5% higher than Cheng's method. Meanwhile, the proposed method demonstrates a more stable and more superior performance than the other two methods, especially when 1/10 of the dataset is treated as the training set. In this case, the proposed method is up to 90.85% on the overall accuracy while the other two methods achieve 81.30% and 81.64%, respectively. That means discriminative features used for classification can be gained even with insufficient training data as well. In Fig. 4, the classification results of the proposed method are demonstrated in the form of the confusion matrix when 1/2 of the dataset constructs the training set while the rest 1/2 is used for testing. Each row of the matrix represents an actual class while each column represents the predicted class given by SVM. For example, the element in the second row and third column is the percentage of cululiform clouds misclassified as waveform clouds. Therefore, the recognition rate for each class is in the diagonal of the matrix. The discrimination rate of stratiform clouds is up to 100%, which indicates that stratiform clouds have the most significant features to be distinguished among five cloud types. Likewise, the results of the other four cloud types achieve over 93%. It is shown that a rather high accuracy of each cloud type has reached, which means the proposed method performs well in classifying the ground-based infrared zenithal images on the whole.

3.2 Results of the whole-sky dataset

The second experiment is performed on the whole-sky dataset, which is more challenging because there exits larger inner-class difference than that of the zenthial dataset. The experimental configuration retains the same in Sec. 3.1. Table 5 lists the results of different methods. It is illustrated that the proposed method gains the overall accuracy of 78.27%, 83.54% and

85.01% as the proportion of the training set varies. In comparison, Liu's method achieves 73.58%, 80.55% and 81.31% while Cheng's method achieves 66.99%, 67.36% and 68.18%, correspondingly. Comparing to the other two methods, the experimental results indicate the effectiveness of the proposed method with an obvious improvement in the accuracy. Figure 5 displays the confusion matrix of the whole-sky dataset when 1/2 for training. The number of each category in the training set is 123, 120, 120, 23 and 44, respectively and the remaining part is treated as the testing set. It is demonstrated that stratiform clouds and clear sky possess obvious characteristics for classification while cumuliform, waveform and cirriform clouds pose a great challenge for a high accuracy of classification. Cirriform clouds are likely to be confused with the clear sky and about 15.22% of cirriform cloud images are misclassified as the clear sky in the experiment. In the whole-sky image, when it is on the condition of cirriform clouds, the area of cirriform clouds may be just a fraction of the whole sky, making it hard to be distinguished correctly. What's more, multiple cloud types could exist in the whole-sky condition, which may result in a relatively low accuracy of the single-type classification, like cumuliform, waveform and cirriform clouds.

There are some misclassifications, just as demonstrated in Fig. 6. Figure 6(a) shows that stratiform clouds are recognized as waveform clouds. It can be seen that the cloud base has a little fluctuation and makes it similar to the waveform cloud. Figure 6(b) shows that cumuliform clouds are recognized as waveform clouds. We can distinguish it as waveform clouds by the shape but the strong vertical motion of cumuliform clouds makes it hard to differ from waveform clouds. Figure 6(c) shows that cumuliform clouds are recognized as cirriform clouds. In this image, besides cumuliform clouds, a little cirriform clouds can also be found. Figure 6(d) shows that waveform clouds are recognized as cumuliform clouds. It can be seen that both waveform and cumuliform clouds coexist in the sky. Figure 6(e) shows that cirriform clouds are recognized as cumuliform clouds. It is admitted that the whole-sky dataset is more complicated than the zenithal dataset as the weather conditions change.

4. Conclusions

In this paper, a novel cloud classification method of the ground-based infrared images, including the zenithal and whole-sky datasets, is proposed. Besides the texture features computed from the GLCM, manifold features obtained from the SPD matrix manifold are combined together. With the joint features, the proposed method can improve the recognition rate of the cloud types dramatically. On the one hand, the joint features can inherit the advantages of the statistical features, which represent texture information in Euclidean space; on the other hand, the statistical learning method on the manifold can describe the non-Euclidean geometric structure of the image features and thus the proposed method can benefit from it for a high classification precision. The CovD is calculated by extracting 6-dimensional features including greyscale, first-order and second-order gradient information, and the mean values are subtracted from the feature vectors, which may improve the recognition performance to some extent, since it can remove the noises of the infrared images. The manifold feature vector is produced by mapping the SPD matrix into the tangent space and afterwards the combined feature vector is adopted for cloud type recognition with SVM. In future work, more suitable image features like Gabor or wavelet coefficients can be incorporated into the SPD matrix and the classification would be performed directly on the manifolds to improve the

recognition rate further. Besides, feature extraction using deep learning method such as convolutional neural networks can be taken into account to increase the classification accuracy. It is found that the proposed method is effective to satisfy the requirement of the cloud classification task on the both zenithal and whole-sky datasets. The complex sky condition with multiple cloud types should arise our concern in the next work.

5. Code availability

The code of the proposed method will be available online upon the acceptance of the paper.

6. Data availability

The two ground-based infrared cloud datasets used in this paper will be available upon the acceptance of the paper. This will be helpful for further benchmarking ground-based infrared image classification.

Acknowledgements. This work is in part supported financially by the National Natural Science Foundation of China under Grant No.61473310 and No.41174164.

References

Arsigny, V., Fillard, P., Pennec, X., and Ayache, N.: Geometric Means In A Novel Vector Space Structure On Symmetric Positive-Definite Matrices, Siam J. Matrix Anal. A., 29, 328-347, doi:10.1137/050637996, 2008.

Bensmail, H., and Celeux, G.: Regularized Gaussian Discriminant Analysis Through Eigenvalue Decomposition, J. Am. Stat. Assoc., 91, 1743-1748, doi:10.1080/01621459.1996.10476746, 1996.

Calbó, J., and Sabburg, J.: Feature Extraction from Whole-Sky Ground-Based Images for Cloud-Type Recognition, J. Atmos. Ocean. Techn., 25, 3, doi:10.1175/2007JTECHA959.1, 2008.

Cazorla, A., Olmo, F. J., and Aladosarboledas, L.: Development of a sky imager for cloud cover assessment, J. Opt. Soc. Am. A., 25, 29-39, doi:10.1364/JOSAA.25.000029, 2008.

Chen, T., Rossow, W. B., and Zhang, Y.: Radiative Effects of Cloud-Type Variations. J. Climate, 13, 264-286, doi: 10.1175/1520-0442(2000)013<0264, 2000.

Cheng, H. Y., and Yu, C. C.: Block-based cloud classification with statistical features and distribution of local texture features, Atmos. Meas. Tech., 7, 1173-1182, doi:10.5194/amt-8-1173-2015, 2015.

Faraki, M., Palhang, M., and Sanderson, C.: Log-Euclidean bag of words for human action recognition, IET Comput. Vis., 9, 331-339, doi:10.1049/iet-cvi.2014.0018, 2015.

Gan, J., Lu, W., Li, Q., Zhang, Z., Yang, J., Ma, Y. and Yao, W.: Cloud type classification of total-sky images using duplex norm-bounded sparse coding. IEEE J. Sel. Top. Appl., 10, 3360-3372, doi:10.1109/JSTARS.2017.2669206, 2017.

Ghonima, M. S., Urquhart, B., Chow, C. W., and Shields, J. E.: A method for cloud detection and opacity classification based on ground based sky imagery, Atmos. Meas. Tech., 5, 4535-4569, doi:10.5194/amt-5-2881-2012, 2012.

Haralick, R. M., Shanmugam, K., and Dinstein, I. H.: Textural Features for Image Classification, IEEE T. Syst. Man Cyb., 3, 610-621, doi:10.1109/TSMC.1973.4309314, 1973.

Harandi, M. T., Hartley, R., Lovell, B., and Sanderson, C.: Sparse Coding on Symmetric Positive Definite Manifolds Using Bregman Divergences, IEEE T. Neur. Net. Lear., 27, 1294-1306, doi:10.1109/TNNLS.2014.2387383, 2015.

Hartmann, D. L., Ockert-bell, M. E., and Michelsen M. L.: The effect of cloud type on earth's energy balance: global analysis. J. Climate., 5, 1281-1304, doi:10.1175/1520-0442(1992)005<1281, 1992.

Heinle, A., Macke, A., and Srivastav, A.: Automatic cloud classification of whole sky images, Atmos. Meas. Tech., 3, 557-567, doi:10.5194/amt-3-557-2010, 2010.

Isaac, G. A., and Stuart, R. A.: Relationships between Cloud Type and Amount, Precipitation, and Surface Temperature in the Mackenzie River Valley-Beaufort Sea Area. J. Climate, 9, 1921-1941, doi:10.1175/1520-0442(1996)<1921, 1996.

Jayasumana, S., Hartley, R., Salzmann, M., Li, H., and Harandi, M.: Kernel Methods on Riemannian Manifolds with Gaussian RBF Kernels, IEEE T. Pattern Anal., 37, 2464-2477, doi:10.1109/TPAMI.2015.2414422, 2015.

Li, J., Menzel, W. P., Yang, Z., Frey, R. A., and Ackerman, S. A.: High-Spatial-Resolution Surface and Cloud-Type Classification from MODIS Multispectral Band Measurements, J. Appl. Meteorol., 42, 204-226, doi:10.1175/1520-0450(2003)042<0204, 2002.

Li, Q., Zhang, Z., Lu, W., Yang, J., Ma, Y. and Yao, W.: From pixels to patches: a cloud classification method based on bag of micro-structures, Atmos. Meas. Tech., 9, 753-764, doi:10.5194/amt-9-753-2016, 2016.

Liu, L., Sun, X., Chen, F., Zhao, S., and Gao, T.: Cloud Classification Based on Structure Features of Infrared Images, J. Atmos. Ocean. Techn., 28, 410-417, doi:10.1175/2010JTECHA1385.1, 2011.

Liu, L., Sun, X., Gao, T., and Zhao, S.: Comparison of Cloud Properties from Ground-Based Infrared Cloud Measurement and Visual Observations, J. Atmos. Ocean. Techn., 30, 1171-1179, doi:10.1175/JTECH-D-12-00157.1, 2013.

Liu, S., Zhang, Z., and Mei, X.: Ground-based cloud classification using weighted local binary patterns, J. Appl. Remote Sens., 9, 095062, doi:10.1117/1.JRS.9.095062, 2015.

Liu, Y., Key, J. R., and Wang, X.: The Influence of Changes in Cloud Cover on Recent Surface Temperature Trends in the Arctic. J. Climate, 21, 705-715, doi: 10.1175/2007JCLI1681.1, 2008.

Naud, C. M., Booth, J. F. and Del Genio, A.D.: The relationships between boundary layer stability and cloud cover in the post-cloud-frontal region. J. Climate, 29, 8129-8149, doi: 10.1175/JCLI-D-15-0700.1, 2016.

Shi, C., Wang, C., Wang, Y., and Xiao, B.: Deep Convolutional Activations-Based Features for Ground-Based Cloud Classification, IEEE Geosci. Remote S., PP, 1-5, doi:10.1109/LGRS.2017.2681658, 2017.

Shields, J. E., Johnson, R. W., Karr, M. E., Burden, A. R., and Baker, J. G.: Daylight visible/NIR whole-sky imagers for cloud and radiance monitoring in support of UV research programs, SPIE International Symposium on Optical Science & Technology, 155-166, doi: 10.1117/12.509062, 2003.

Singh, M., and Glennen, M.: Automated ground-based cloud recognition, Pattern Anal. Appl., 8, 258-271, doi: 10.1007/s10044-005-0007-5, 2005.

Souzaecher, M. P., Pereira, E. B., Bins, L. S., and Andrade, M. A. R.: A Simple Method for the Assessment of the Cloud Cover State in High-Latitude Regions by a Ground-Based Digital Camera, J. Atmos. Ocean. Techn., 23, 437, doi: 10.1175/JTECH1833.1, 2006.

Sun, X. J., Liu, L., Gao, T. C., and Zhao, S. J.: Classification of Whole Sky Infrared Cloud Image Based on the LBP Operator, Transactions of Atmospheric Sciences, 32, 490-497, doi:10.3969/j.issn.1674-7097.2009.04.004, 2009 (in Chinese).

Taravat, A., Frate, F. D., Cornaro, C., and Vergari, S.: Neural Networks and Support Vector Machine Algorithms for Automatic Cloud Classification of Whole-Sky Ground-Based Images, IEEE Geosci. Remote S., 12, 666-670, doi:10.1109/LGRS.2014.2356616, 2014.

Tzoumanikas, P., Kazantzidis, A., Bais, A. F., Fotopoulos, S., and Economou, G.: Cloud Detection and Classification with the Use of Whole-Sky Ground-Based Images, Atmos. Res., 113, 80-88, doi:10.1016/j.atmosres.2012.05.005, 2012.

Wang, Z., and Sassen, K.: Cloud Type and Macrophysical Property Retrieval Using Multiple Remote Sensors, J. Appl. Meteorol., 40, 1665-1683, doi:10.1175/1520-0450(2001)040<1665, 2001.

Zhuo, W., Cao, Z., and Xiao, Y.: Cloud Classification of Ground-Based Images Using Texture–Structure Features, J. Atmos. Ocean. Techn., 31, 79-92, doi:10.1175/JTECH-D-13-00048.1, 2014.

Atmos. Meas. Tech. Discuss., https://doi.org/10.5194/amt-2017-402
Manuscript under review for journal Atmos. Meas. Tech.
Discussion started: 22 December 2017

Atmospheric Measurement Techniques Discussions

Table 1. The sky condition classes and corresponding description.

Sky condition classes	Description	Cloud types
Stratiform clouds	Horizontal, layered clouds that stretch out across the sky like a blanket	St、As、Cs (Sc、Ac、Cb、Ns)
Cumuliform clouds	Thick clouds that are puffy in appearance, like large cotton balls	Cu、Cb
Waveform clouds	Thin or thick clouds occurring in sheets or patches with wavy, rounded masses or rolls	Sc、Ac、Cc
Cirriform clouds	Thin clouds; very wispy and feathery looking	Ci
Clear sky	Clear	No clouds

Atmos. Meas. Tech. Discuss., https://doi.org/10.5194/amt-2017-402
Manuscript under review for journal Atmos. Meas. Tech.
Discussion started: 22 December 2017

Atmospheric Measurement Techniques Discussions

Table 2. The numbers of each class on two datasets.

Sky condition classes	Zenithal	Whole-sky
Stratiform clouds	100	246
Cumuliform clouds	100	240
Waveform clouds	100	239
Cirriform clouds	100	46
Clear sky	100	88
Total	500	859

Atmos. Meas. Tech. Discuss., https://doi.org/10.5194/amt-2017-402
Manuscript under review for journal Atmos. Meas. Tech.
Discussion started: 22 December 2017

Atmospheric Measurement Techniques Discussions

Table 3. The 10-fold cross validated classification accuracy (%) on two datasets.

	Zenithal	Whole-sky
Texture features	83.49	78.01
Manifold features	96.46	82.38
Combined features	**96.50**	**85.12**

Atmos. Meas. Tech. Discuss., https://doi.org/10.5194/amt-2017-402
Manuscript under review for journal Atmos. Meas. Tech.
Discussion started: 22 December 2017

Atmospheric Measurement Techniques Discussions

Table 4. The overall classification accuracy (%) on the zenithal dataset.

	1/10	1/2	9/10
Liu's method	81.64	92.24	93.48
Cheng's method	81.30	81.92	81.32
Proposed method	**90.85**	**95.98**	**96.36**

Atmos. Meas. Tech. Discuss., https://doi.org/10.5194/amt-2017-402
Manuscript under review for journal Atmos. Meas. Tech.
Discussion started: 22 December 2017

Atmospheric Measurement Techniques Discussions

Table 5. The overall classification accuracy (%) on the whole-sky dataset.

	1/10	1/2	9/10
Liu's method	73.58	80.55	81.31
Cheng's method	66.99	67.36	68.18
Proposed method	**78.27**	**83.54**	**85.01**

Atmos. Meas. Tech. Discuss., https://doi.org/10.5194/amt-2017-402
Manuscript under review for journal Atmos. Meas. Tech.
Discussion started: 22 December 2017

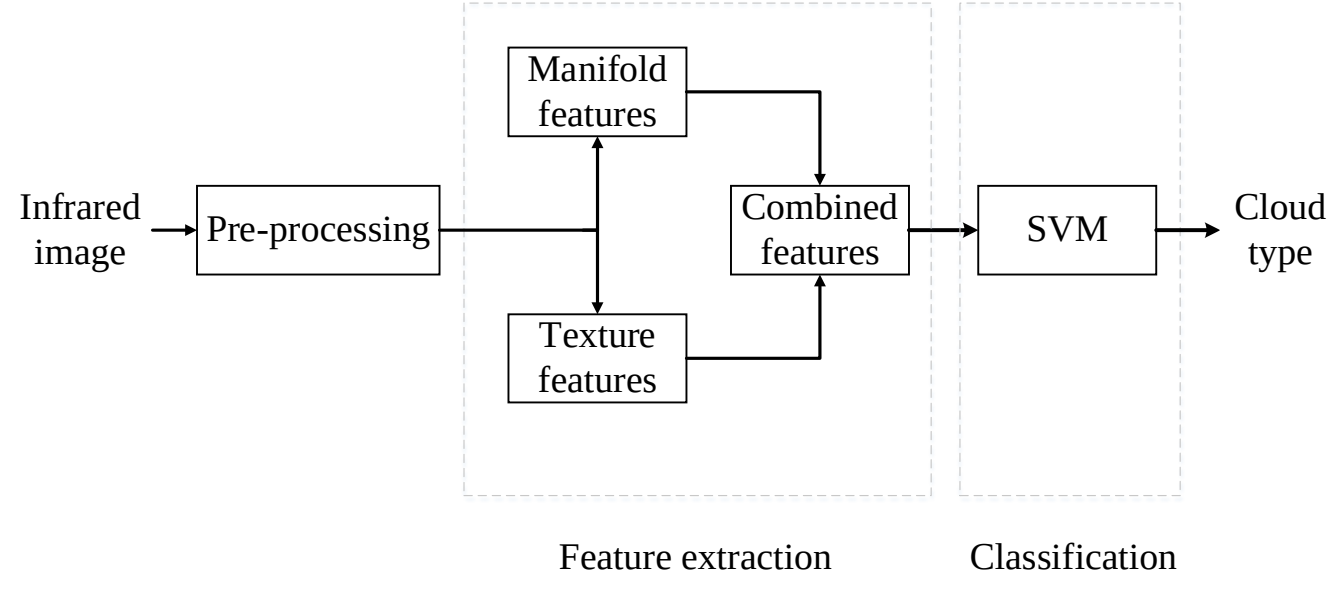

Figure 1: System framework.

Atmos. Meas. Tech. Discuss., https://doi.org/10.5194/amt-2017-402
Manuscript under review for journal Atmos. Meas. Tech.
Discussion started: 22 December 2017

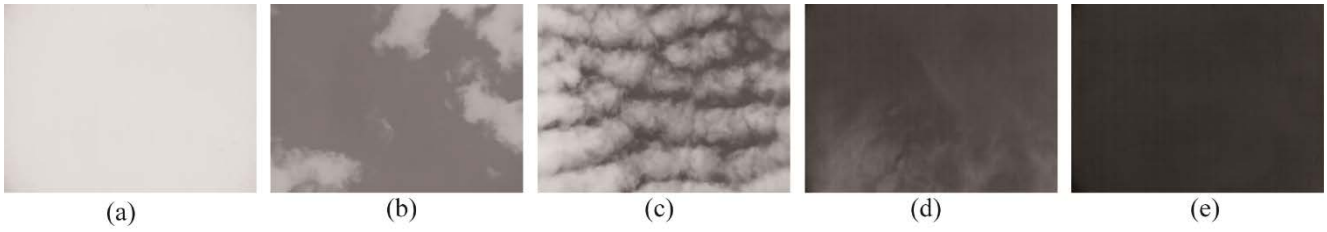

Figure 2: Cloud samples from the zenithal dataset. (a) stratiform clouds, (b) cumuliform clouds, (c) waveform clouds, (d) cirriform clouds and (e) clear sky.

Atmos. Meas. Tech. Discuss., https://doi.org/10.5194/amt-2017-402
Manuscript under review for journal Atmos. Meas. Tech.
Discussion started: 22 December 2017

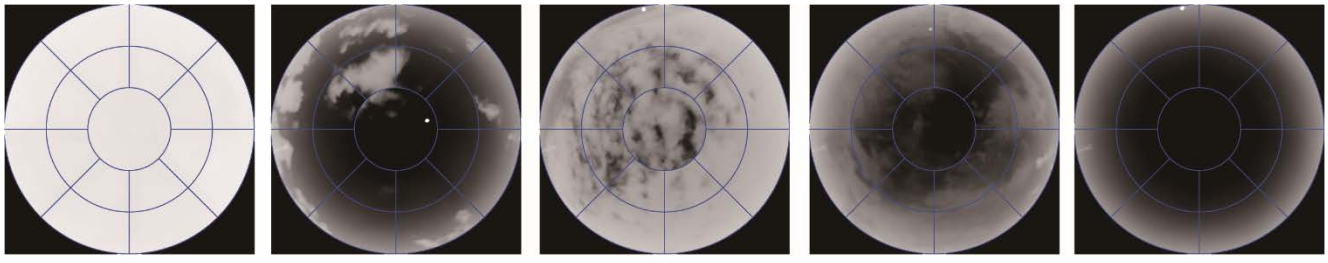

Figure 3: Cloud samples from the whole-sky dataset. (a) stratiform clouds, (b) cumuliform clouds, (c) waveform clouds, (d) cirriform clouds and (e) clear sky.

Atmos. Meas. Tech. Discuss., https://doi.org/10.5194/amt-2017-402
Manuscript under review for journal Atmos. Meas. Tech.
Discussion started: 22 December 2017

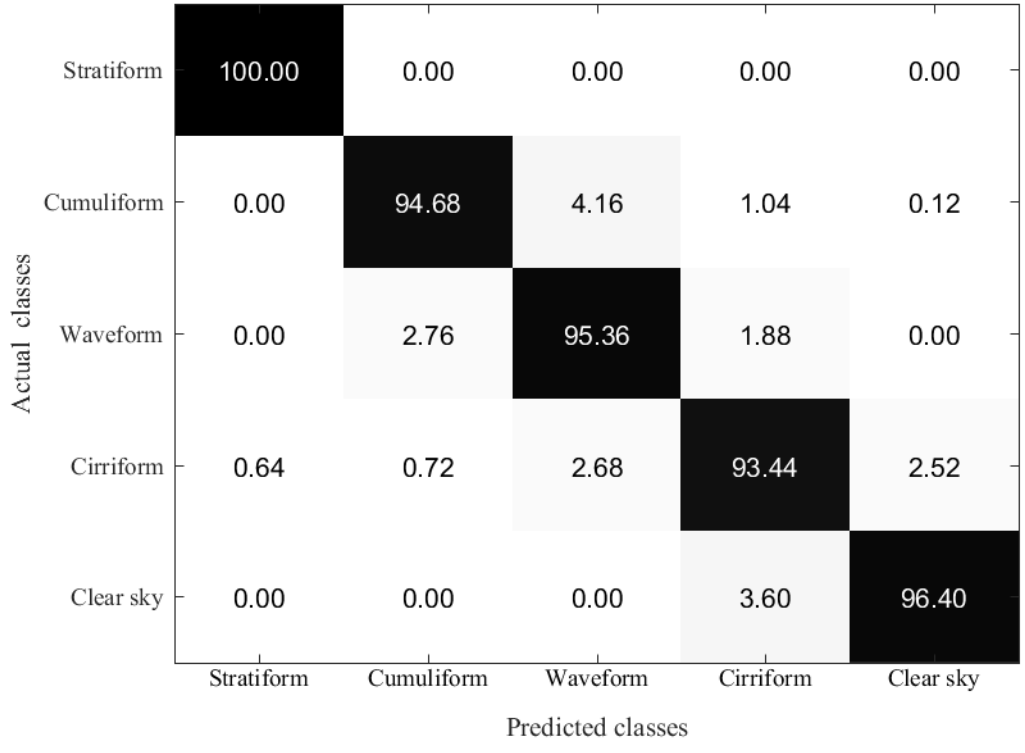

Figure 4: Confusion matrix (%) on the zenithal dataset. (1/2 for training and the overall accuracy is 95.98%)

Atmos. Meas. Tech. Discuss., https://doi.org/10.5194/amt-2017-402
Manuscript under review for journal Atmos. Meas. Tech.
Discussion started: 22 December 2017

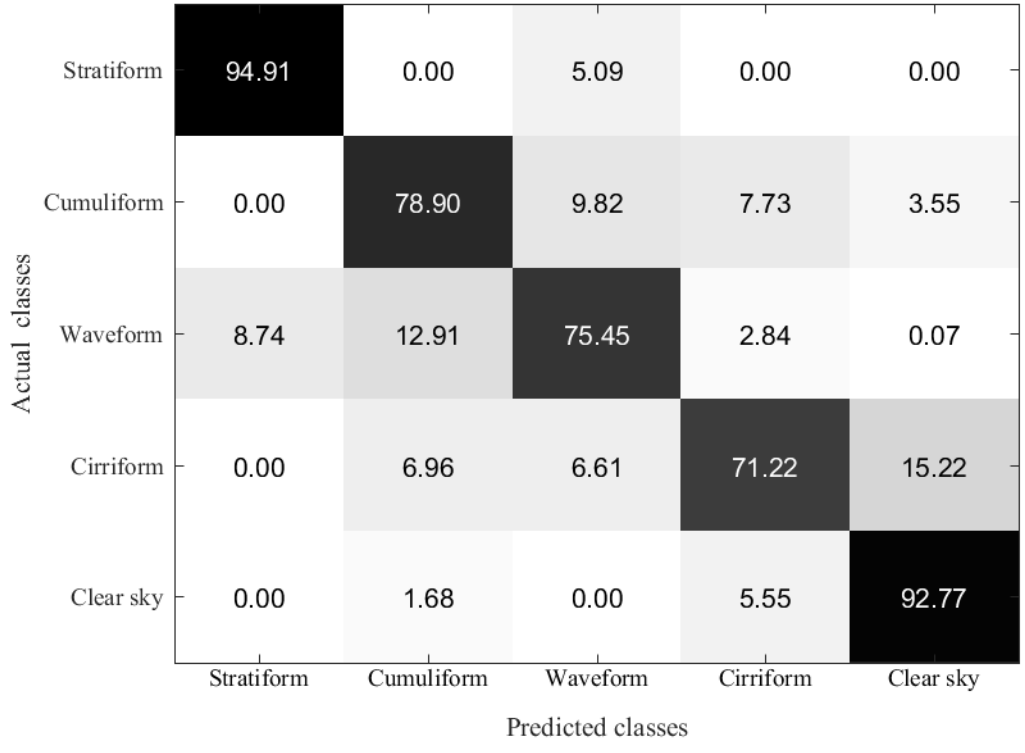

Figure 5: Confusion matrix (%) on the whole-sky dataset. (1/2 for training and the overall accuracy is 83.54%)

Atmos. Meas. Tech. Discuss., https://doi.org/10.5194/amt-2017-402
Manuscript under review for journal Atmos. Meas. Tech.
Discussion started: 22 December 2017

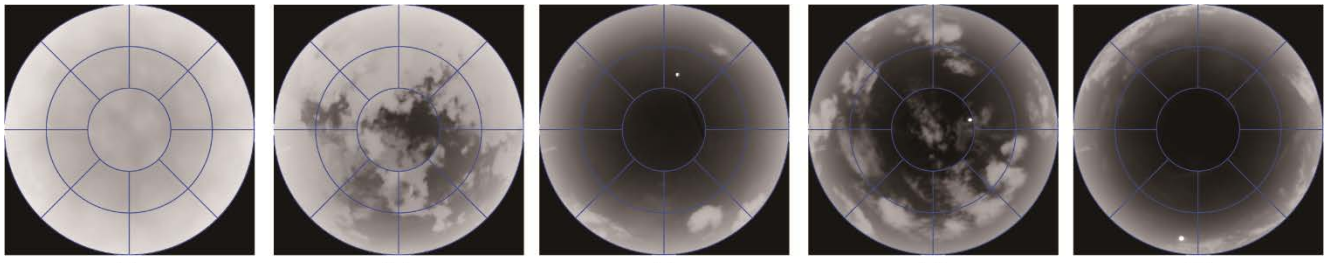

Figure 6: Selected misclassified whole-sky images. (a) stratiform clouds to waveform clouds, (b) cumuliform clouds to waveform clouds, (c) cumuliform clouds to cirriform clouds, (d) waveform clouds to cumuliform clouds and (e) cirriform clouds to cumuliform clouds.